Sedimentary Geology 341 (2016) 134–146

Contents lists available at ScienceDirect

Sedimentary Geology

journal homepage: www.elsevier.com/locate/sedgeo

Phosphogenesis associated with the Shuram Excursion: Petrographic and geochemical observations from the Ediacaran Doushantuo Formation of South China

Huan Cui [a,b,*], Shuhai Xiao [c], Chuanming Zhou [d], Yongbo Peng [e], Alan J. Kaufman [b,f], Rebecca E. Plummer [b]

[a] Department of Geoscience and NASA Astrobiology Institute, University of Wisconsin-Madison, Madison, WI 53706, USA
[b] Department of Geology, University of Maryland, College Park, MD 20742, USA
[c] Department of Geosciences, Virginia Tech, Blacksburg, VA 24061, USA
[d] Key Laboratory of Economic Stratigraphy and Palaeogeography, Nanjing Institute of Geology and Palaeontology, Chinese Academy of Science, Nanjing 210008, China
[e] Department of Geology and Geophysics, Louisiana State University, Baton Rouge, LA 70803, USA
[f] Earth System Science Interdisciplinary Center, University of Maryland, College Park, MD 20742, USA

ARTICLE INFO

Article history:
Received 13 March 2016
Received in revised form 9 May 2016
Accepted 10 May 2016
Available online 18 May 2016

Editor: Dr. B. Jones

Keywords:
Phosphogenesis
Sulfate–methane transition zone
Microbial sulfate reduction
Authigenic carbonates
Shuram Excursion
C-S-P-Fe cycles

ABSTRACT

The Ediacaran Period witnessed one of the largest phosphogenic events in Earth's history. Coincidently, some phosphorite deposits in South China are associated with the largest-known carbon isotope negative excursion (i.e., Shuram Excursion), suggesting an intimate coupling of the biogeochemical carbon and phosphorous cycles. However, the geomicrobiological linkage between these anomalies remain poorly understood. In this study, we investigated the phosphorite samples from the uppermost Doushantuo Formation in South China. Carbon isotope compositions of authigenic calcite cements and nodules in the phosphorites are as low as −34‰ (VPDB). Petrographic and geochemical investigations indicate that the ^{13}C-depleted carbonates likely formed as the result of microbial sulfate and iron reduction that released phosphorous from iron oxyhydroxide, concentrating phosphorous in pore waters, and thereby promoting phosphate mineralization. The timing of this event appears to coincide with enhanced sulfate delivery to seawater through continental weathering. The basin-scale distribution of Doushantuo phosphorites suggests a redox control on the availability of iron oxyhydroxide and the recycling of pore water phosphorous. Both inner and outer shelf regions were likely characterized by an oxic water column, and were the main loci for phosphogenesis; on the contrary, intra-shelf and slope regions, which are lean in phosphorite, were subjected to euxinic or ferruginous water column conditions. The intimate coupling between Ediacaran phosphogenesis and the Shuram Excursion suggests strong links among seawater redox conditions, C-S-P-Fe cycling, and fossil phosphatization. Increased microbial sulfate reduction driven by enhanced sulfate reservoir in the Ediacaran ocean may have played an essential role on these biogeochemical events.

1. Introduction

Phosphorus, a nonmetal element and bio-limiting nutrient, is relatively rare but vastly important to marine primary productivity (Tyrrell, 1999). Fluctuations in phosphorous cycling in the oceans on geological time scales are thought to be intimately linked to the global carbon cycle, atmospheric oxygenation, and biological evolution (Brasier, 1992; Saltzman, 2005; Planavsky et al., 2010). In this regard, the sedimentary record of phosphorite may be used to interpret variations in biological productivity at geological timescales (Mort et al., 2007; Paytan and McLaughlin, 2007; Diaz et al., 2008). In addition, phosphorites offer an exceptional taphonomic window for extraordinary preservation of soft-bodied organisms in the Ediacaran Period (Martill and Wilby, 1994; Xiao and Knoll, 1999; Schiffbauer et al., 2014; Zhang et al., 2015) and small shelly fossils in the Early Cambrian (Dzik, 1994; Porter, 2004; Creveling et al., 2014). In particular, phosphatization is responsible for the preservation of a significant portion of Ediacaran biodiversity that is documented in the literature (Xiao et al., 2014a; Muscente et al., 2015).

Despite intensive research on modern phosphorites (e.g., Arning et al., 2009), much less is known about how phosphorites in deep time were formed. The Ediacaran and Early Cambrian periods witnessed a series of widespread phosphogenic events that stand out in Earth history (Cook and Shergold, 1984; Cook, 1992; Papineau, 2010). However, our understanding of the origin of these phosphorites remains incomplete. In South China, Ediacaran and Cambrian phosphorites are widely distributed and richly fossiliferous (Li, 1986; Yeh et al., 1986; Muscente et al., 2015). Three-dimensionally phosphatized microfossils,

* Corresponding author at: Department of Geoscience and NASA Astrobiology Institute, University of Wisconsin-Madison, Madison, WI 53706, USA.
E-mail address: Huan.Cui@Wisc.EDU (H. Cui).

http://dx.doi.org/10.1016/j.sedgeo.2016.05.008
0037-0738/

including acritarchs (Zhou et al., 2001; Xiao et al., 2014b), multicellular algae (Xiao et al., 2004), and putative animals (Xiao et al., 1998, 2014a; Yin et al., 2015) have been reported from phosphorites of the Ediacaran Doushantuo Formation in Guizhou Province. Phosphatized animals, including cnidarians and early scalidophorans, have been reported from phosphorites of the early Cambrian Kuanchuanpu Formation of Shaanxi and Sichuan provinces (Dong et al., 2004, 2013; Liu et al., 2014b; Zhang et al., 2015). Thus, a better understanding of Ediacaran phosphogenesis provides insights into the taphonomy of early animals across the Ediacaran–Cambrian transition.

It has long been speculated that phosphorous enrichment in pore waters for authigenic carbonate fluorapatite mineralization is achieved by organic carbon degradation (Glenn and Arthur, 1990; Filippelli, 2001, 2008). Previous studies in modern settings have shown that degradation of organic matter via microbial sulfate and iron reduction is the predominant anaerobic respiration process in marine sediments (Jørgensen, 1982; Thamdrup and Canfield, 1996; Jørgensen and Kasten, 2006). However, conclusive evidence linking microbial sulfate and iron reduction and Ediacaran phosphogenesis is lacking. In this study, we conducted systematic petrographic and isotopic investigation of phosphorite samples collected from the uppermost Doushantuo Formation at the outer shelf Yangjiaping and Zhongling sections, and provide direct geological evidence for microbially-mediated phosphogenesis during the Ediacaran Period.

2. Geological background

Ediacaran successions in the Yangtze block of South China include the richly fossiliferous Doushantuo and Dengying formations (Fig. 1A, B). Abundant three-dimensionally preserved eukaryotes, including multicellular algae, acritarchs, and putative animals, have been discovered from phosphorites and chert nodules of the Doushantuo Formation (Xiao et al., 1998; Liu et al., 2014a; Xiao et al., 2014b), while the Dengying Formation contains macroscopic Ediacaran body and trace

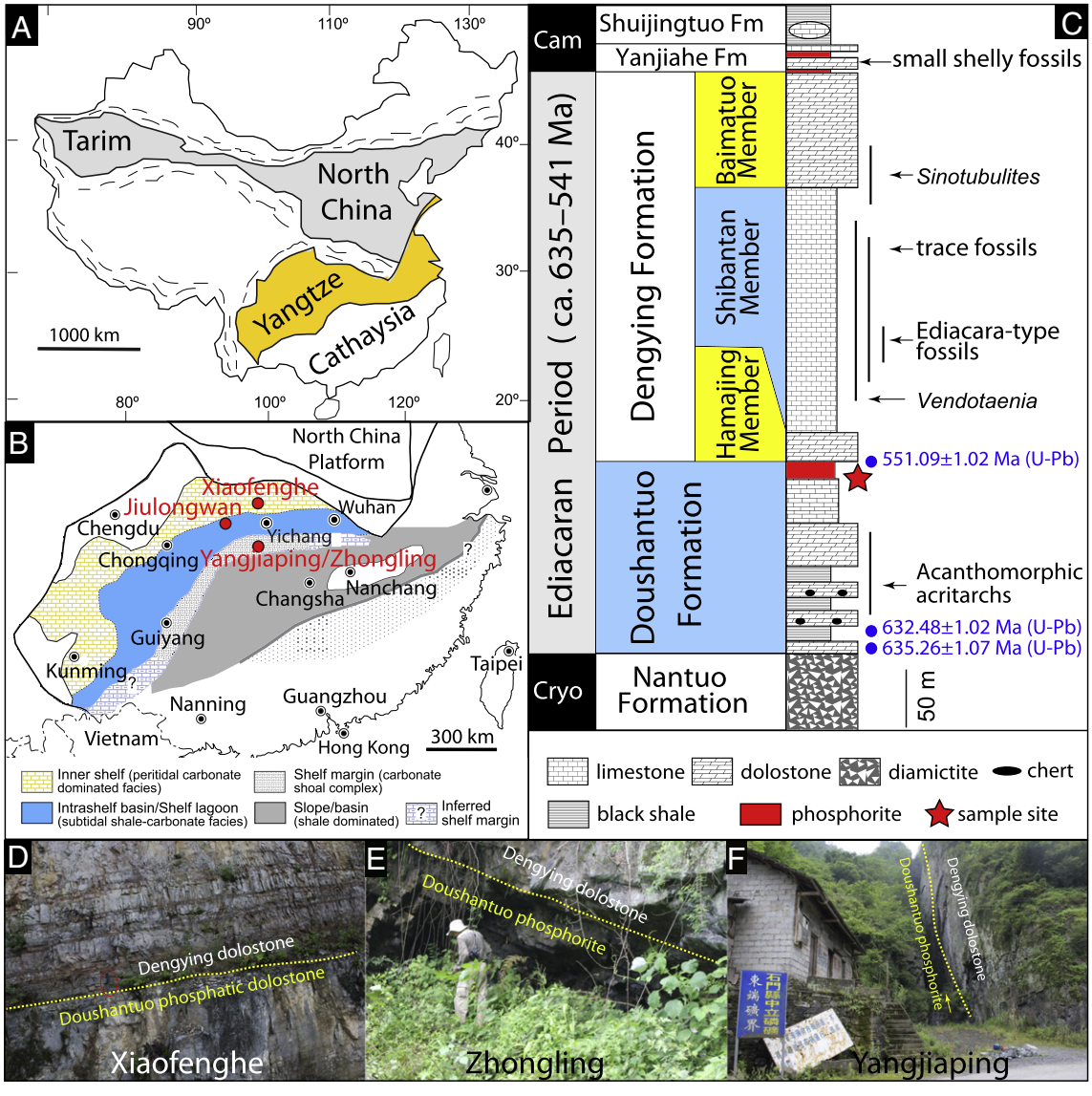

Fig. 1. (**A**) Simplified map of China, showing the location of the Yangtze Craton (in yellow color). (**B**) Reconstructed Ediacaran depositional environments on the Yangtze Craton (Jiang et al., 2011). Red dots mark the locations of the Yangjiaping and Zhongling sections where samples for this study were collected, and the Jiulongwan section as a reference section for stratigraphic correlation. (**C**) Simplified litho-, bio-, and chrono-stratigraphy of the Ediacaran Doushantuo and Dengying formations in South China. Modified from Chen et al. (2013). Radiometric ages from Condon et al. (2005) and Schmitz (2012). The red star marks the stratigraphic horizon where samples for this study were collected. (**D, E, F**) Phosphatic dolostone in the uppermost Doushantuo Formation at the southern Xiaofenghe, Zhongling, and Yangjiaping sections, respectively. Rock hammer for scale is circled. Phosphorite intervals at both Zhongling and Yangjiaping sections are 2–3 m in thickness, and they are mined by local villagers (hence the open mine pit in Fig. 1E–F). Cryo = Cryogenian; Cam = Cambrian.

fossils, including the earliest biomineralizing animals (Xiao et al., 2005; Chen et al., 2013, 2014; Meyer et al., 2014; Cui et al., in press). The basal Doushantuo Formation overlies the Nantuo diamictite and begins with a ca. 635 Ma cap carbonate (Condon et al., 2005). It has been suggested that the uppermost Doushantuo Formation corresponds to ca. 551 Ma (Condon et al., 2005), but based on a recent litho- and chemo-stratigraphic study, the age constraint has been attributed to the lower Dengying Formation, thereby pushing the Doushantuo–Dengying boundary (and the Shuram Excursion preserved there) back in time (An et al., 2015). In the Yangtze Gorges area, the Doushantuo Formation is informally divided into four distinct members (Zhou and Xiao, 2007; McFadden et al., 2008) and is typically capped by black shale below the massive dolostones of the Dengying Formation (Zhu et al., 2007; Jiang et al., 2011; Zhu et al., 2013). The mixed shale and carbonate in the inner shelf Jiulongwan section, which is well exposed along a road cut during the construction of the Yangtze Gorges Dam, has a thickness of ~160 m (Jiang et al., 2007; McFadden et al., 2008). In contrast, the carbonate-rich outer shelf sections at Zhongling and Yangjiaping have thicknesses of 215 and 185 m, respectively (Zhu et al., 2007; Jiang et al., 2011; Cui et al., 2015). The Doushantuo Formation, deposited in continental slope and basinal environments further to the southeast, is significantly thinner, and dominated by fine-grained siliciclastics intercalated with thin carbonate inter-beds (Jiang et al., 2007; Zhu et al., 2007).

Deposition of the Doushantuo Formation can be divided into two stages, beginning with an open ramp shelf that gradually transitioned into a rimmed shelf protecting an intra-shelf lagoon (Jiang et al., 2011). Stratigraphic data and paleogeographic reconstructions indicate an increase in water depth from proximal intertidal environments in the northwest to distal deep basinal settings in the southeast. Three platform facies belts are apparent, including a proximal inner shelf dominated by peritidal carbonates, an intra-shelf lagoon containing mixed carbonates and shales, and an outer shelf shoal complex (Fig. 1B). The Doushantuo Formation at the Zhongling section is representative of the shoal complex facies, as is the Yangjiaping section some 4 km to the northeast. At Zhongling and Yangjiaping, the Doushantuo Formation is mainly composed of interbedded shales and carbonates, with an up-section increase in the preponderance of intraclastic and oolitic facies, indicating relatively shallow and high-energy depositional environments (Cui et al., 2015). The upper Doushantuo Formation in the shoal complex contains several phosphorite intervals that occur just below the overlying Dengying Formation (Jiang et al., 2007, 2011; Kunimitsu et al., 2011), which is characterized by massive dolostone deposited in peritidal environments (Duda et al., 2015) (Fig. 1C).

3. Analytical methods

3.1. Carbonate carbon and oxygen isotope analyses

Powders for $\delta^{13}C_{carb}$ and $\delta^{18}O_{carb}$ analyses were collected on polished slabs using a press microdrill. Microdrilling was guided by petrographic fabrics so that different fabrics (e.g., cements, intraclasts, micritic matrix, and carbonate nodules) were sampled separately, in order to characterize the isotopic signatures of different stages of diagenesis. Carbonate $\delta^{13}C_{carb}$ and $\delta^{18}O_{carb}$ were measured by GasBench coupled with Thermo Finnigan Delta V Plus in the Department of Geological Sciences at Indiana University or by a MultiFlow reaction inlet system in-line with an Elementar Isoprime. In either case, samples were loaded into 3.7 ml Labco Exetainer vials and sealed with rubber septa were flushed with 99.999% Helium and manually acidified at 72 °C. The carbon dioxide analyte gas was transferred from the Exetainer head space by an automated needle in a stream of ultra-pure He gas, separated by gas chromatography, and water removed with a Nafion trap, prior to its introduction to the source of the stable isotope mass spectrometers. Isotopic results are expressed in the delta notation as per mil (‰) deviations from the V-PDB standard. Precision for $\delta^{13}C_{carb}$ is routinely better than 0.1‰, and for $\delta^{18}O_{carb}$ is routinely better than 0.3‰.

3.2. Organic matter carbon isotope analysis

Samples for $\delta^{13}C_{org}$ analysis were prepared from bulk samples. Approximately 10 g of sample trimmed with a rock saw to remove weathered surfaces and secondary veins was crushed to 200 mesh and finer, and then repeatedly acidified with 3 M HCl and washed with ultra-pure (18 MΩ) Milli-Q water until the solution reached neutral pH. Decalcified residues were dried overnight and quantified to determine carbonate percentages, and then accurately weighed and folded into small tin cups for combustion in a Eurovector elemental analyzer. The CO_2 released during combustion was separated from other gases with a 3-m stainless steel GC column heated to 60 °C. Organic carbon isotope compositions were measured by an Elementar Isoprime isotope ratio mass spectrometer in the Paleoclimate Co-Laboratory in the Department of Geology at the University of Maryland. Isotopic results are expressed in the delta notation as per mil (‰) deviations from the Vienna Pee Dee Belemnite (V-PDB) standard. Two urea standards were measured between each set of 10 samples and uncertainties for each analytical session based on these standard analyses were determined to be better than 0.1‰.

3.3. Strontium isotope analysis

Aliquots of micro-drilled powders taken from calcite nodules were used in $^{87}Sr/^{86}Sr$ analyses. Approximately 10 mg of powder was sequentially leached (3×) in 0.2 M ammonium acetate (pH ~ 8.2) to remove exchangeable Sr from non-carbonate minerals, and then rinsed (3×) with ultra-pure Milli-Q water. The leached powder was centrifuged, decanted, and acidified with doubly distilled 0.5 M acetic acid overnight to remove strontium from the carbonate crystal structure. The supernatant was centrifuged to remove insoluble residues and then decanted, dried, and subsequently dissolved in 200 μl of 3 M HNO_3. Strontium separation by cation exchange was carried out using a small polyethylene column containing ~1 cm of Eichrom® Sr spec resin. The column was rinsed with 400 μl of 3 M HNO_3 before the dissolved sample was loaded onto the column. After loading, the sample was sequentially eluted with 200 μl of 3 M HNO_3, 600 μl of 7 M HNO_3, and 100 μl of 3 M HNO_3 to remove the Ca, Rb and REE fractions; the Sr fraction adsorbs strongly to the resin in an acidic environment. The Sr fraction was removed by elution with ~800 μl of 0.05 M HNO_3 and the resultant eluate was collected and dried. Approximately 200–300 ng of the dried sample was transferred onto a degassed and pre-baked (~4.2 A under high vacuum) high purity Re filament with 0.7 μl of Ta_2O_5 activator. The prepared filaments were measured using the VG Sector 54 thermal ionization mass spectrometer in the TIMS facility of the University of Maryland Geochemistry Laboratories. Filaments were transferred to a sample carousel, heated under vacuum ($\sim 10^{-7}$ to 10^{-8} atm) to a temperature between 1450 °C and 1650 °C, and analyzed when a stable signal (>1.0 V) was detected on the mass 88 ion beam. Approximately 100 $^{87}Sr/^{86}Sr$ ratios were collected for each sample. Final data have been corrected for fractionation using the standard value $^{86}Sr/^{88}Sr = 0.1194$. The fraction of ^{87}Sr resulting from in situ decay from ^{87}Rb was removed by measurement of rubidium abundance at mass 85. Repeated analysis of the NBS SRM987 standard yields an average value of $^{87}Sr/^{86}Sr = 0.710245 \pm 0.000011$ (2σ) during the analytical window.

4. Petrography and paragenesis

In this study, detailed petrographic investigations (Figs. 2, 3) have been conducted on phosphorite samples collected from the uppermost Doushantuo Formation at Yangjiaping and Zhongling of South China. The phosphorite samples contain abundant phosphatic grains and

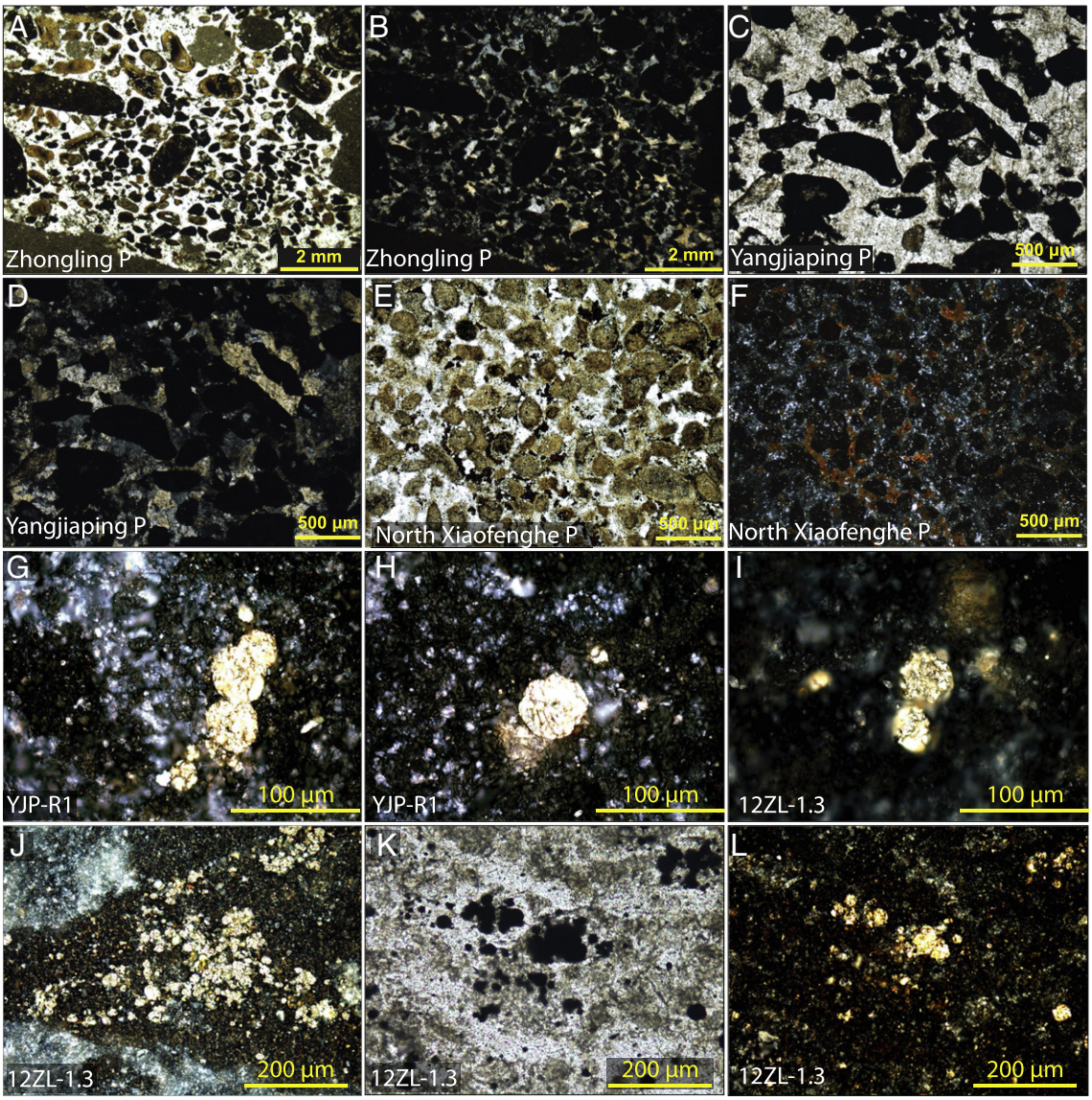

Fig. 2. Microscopic photographs of phosphorite samples from the uppermost Doushantuo Formation. (**A, B**) Intraclastic phosphorite with calcite cements, sample 12ZL-40.9, Zhongling section. (**C, D**) Intraclastic phosphorite with calcite cement, sample Yd-26, Yangjiaping section. (**E, F**) Intraclastic phosphorite with calcite cement, sample NXF-20.3, north Xiaofenghe section. (**G–L**) Disseminated authigenic pyrite in phosphorite samples. (A–F) are paired plane polarized light (PPL) and cross polarized light (XPL) microscopic images, (G–J, L) are reflected light microscopic images, and (K) is a PPL image.

intraclasts, as well as authigenic calcite, barite, and silica. The presence of phosphatic intraclasts (Fig. 2A–F) suggests active sediment reworking in shallow marine environments. Authigenic pyrite is abundant in the phosphorite samples (Fig. 2G–L). Some samples also show distinct barite cements (Fig. 3A–C), calcite nodules (Fig. 3G–J), and authigenic silica (Fig. 3D, G, H, J). Many samples are composed of partially dolomitized (Fig. 3E) or silicified (Fig. 3F) intraclastic phosphorite, suggesting multiple stages of diagenesis. It is notable that authigenic calcite nodules are mostly surrounded by a silica or barite rim (Fig. 3G–J). The barite or silica crystals grow centripetally towards the calcite nodule, suggesting that they formed before or simultaneously with the calcite (e.g., Xiao et al., 2010).

We additionally conducted cathodoluminescence (CL) imaging for our thin sections. Authigenic calcites and silica generally show very dim color under CL light (Fig. 3M), indicating low Mn/Fe concentration ratio. Dolomitic cements around the granular phosphorite show bright orange color (Fig. 3N), suggesting an enrichment of Mn relative to Fe during late dolomitization. Many granular phosphorite grains show concentric texture (Fig. 3O), indicating accretionary growth.

Based on the above petrographic observations, we reconstruct the paragenetic sequence as the following: (1) Dissolved phosphate in the water column was transported to the marine sediments via the "Fe–P shuttle" (Shaffer, 1986; Glenn et al., 1994; Nelson et al., 2010). The release of Fe-bound phosphorous after deposition raised the porewater supersaturation levels with regard to phosphate, leading to the precipitation of authigenic phosphate. (2) The abundance of phosphatic intraclasts suggests that Doushantuo phosphorite experienced sedimentary reworking and local transportation. (3) After final deposition, phosphatic intraclasts were cemented by authigenic barite, calcite, pyrite and silica. (4) Late dolomitization and pyrite recrystallization may also occur in some samples. Thus, these studied Doushantuo phosphorite samples recorded multiple stages of reworking and mineralization during early and late diagenesis.

5. Geochemical results

$\delta^{13}C_{carb}$, $\delta^{18}O_{carb}$, $\delta^{13}C_{org}$, and $^{87}Sr/^{86}Sr$ data are presented along with photos of polished slabs in Fig. 4 and summarized in Table 1. In sample YJP-R5 (Fig. 4A, B), four micro-drilled powder samples from calcite

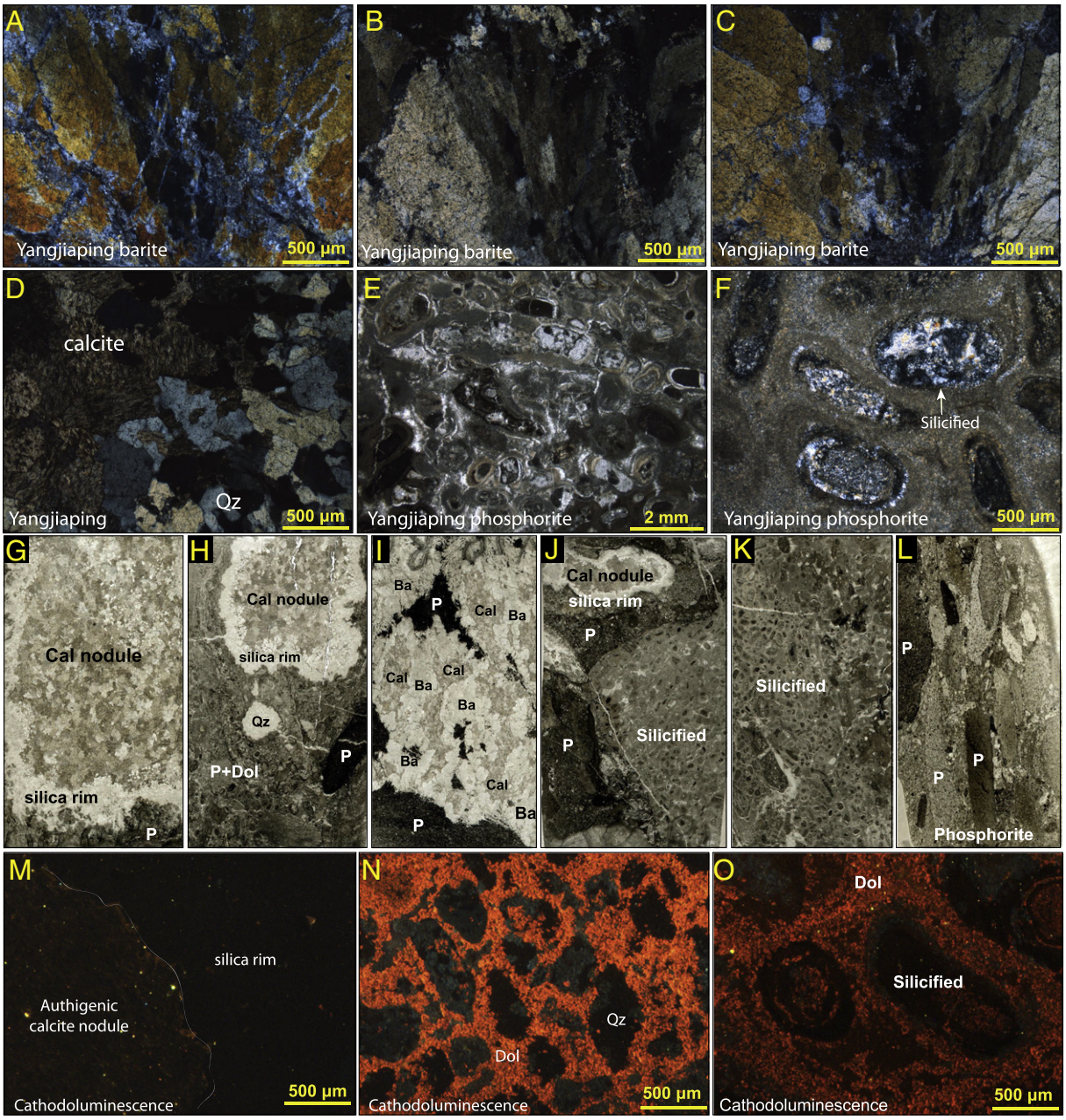

Fig. 3. Petrographic observations of phosphorite samples collected from the uppermost Doushantuo Formation at the Yangjiaping section. **(A–C)** XPL images of barite crystals. **(D)** XPL image of authigenic silica (Qz) and calcite. (**E**) PPL image of granular phosphorite. **(F)** XPL image of silicified phosphorite granules. **(G–L)** Scanned thin section photos, showing **(G–H)** large calcite nodules (Cal) with silica rims (Qz), **(I)** calcite nodules with barite rim (Ba). Note that the barite or silica crystals grow centripetally towards the calcite nodule, suggesting that they formed before or simultaneously with the calcite. **(J–K)** silicified phosphorite granules, and **(L)** large phosphatic intraclasts (P). (**M–O**) Cathodoluminescence (CL) images showing authigenic calcite nodules, authigenic silica rim (Qz rim), dolomitic cements (Dol), and silicified phosphorite granules with concentric fabrics.

nodules gave $\delta^{13}C_{carb}$ values (−15.0‰, −10.6‰, −19.1‰, −20.1‰) significantly lower than the dolomicritic matrix (−1.0‰). Sample YJP-R4 shows both authigenic barite and authigenic calcite nodules in phosphorite (Fig. 4C, D). The $\delta^{13}C_{carb}$ value of a calcite nodule in YJP-R4 is as low as −34.0‰. In the intraclastic phosphorite sample YJP-10-2 (Fig. 4E, F), authigenic calcite nodules and disseminated pyrites are abundant, and the $\delta^{13}C_{carb}$ values of calcite nodules are −7.3‰, −13.1‰, −17.0‰, −17.7‰, and −23.5‰ at different micro-drilled spots. In sample YJP-R9 (Fig. 4H), dolomitic matrix has $\delta^{13}C_{carb}$ and $\delta^{18}O_{carb}$ values around −0.6‰ and −4.9‰, respectively; on the contrary, micro-drilled powders from intraclastic phosphorites (with carbonate cements) reveal much more negative values of −10.6‰ and −7.7‰ for $\delta^{13}C_{carb}$ and $\delta^{18}O_{carb}$ compositions, respectively.

Similar to the Yangjiaping samples, phosphorite samples 12ZL-1.3 (Fig. 4G), 12ZL-4.5 (Fig. 4I), and 12ZL-0.9 (Fig. 4J) collected from the Zhongling section also show significant heterogeneity in $\delta^{13}C_{carb}$ compositions. Typically, calcite phases are remarkably depleted in ^{13}C compared with the phosphatic or dolomitic matrix. In the phosphorite sample YJP-R1 (Fig. 4K), $\delta^{13}C_{carb}$ value of the dolomitic matrix is +1.2‰, in contrast with strongly negative values measured from authigenic calcite nodules in all the phosphorite samples.

Carbonate oxygen isotope compositions show a narrow range of variation. In general, $\delta^{18}O_{carb}$ values of calcite nodules are slightly lower than that of dolomitic matrix or cements in intraclastic phosphorite. Organic C isotope compositions of decalcified bulk powder measured from our samples range from −24.3‰ to −28.6‰. We

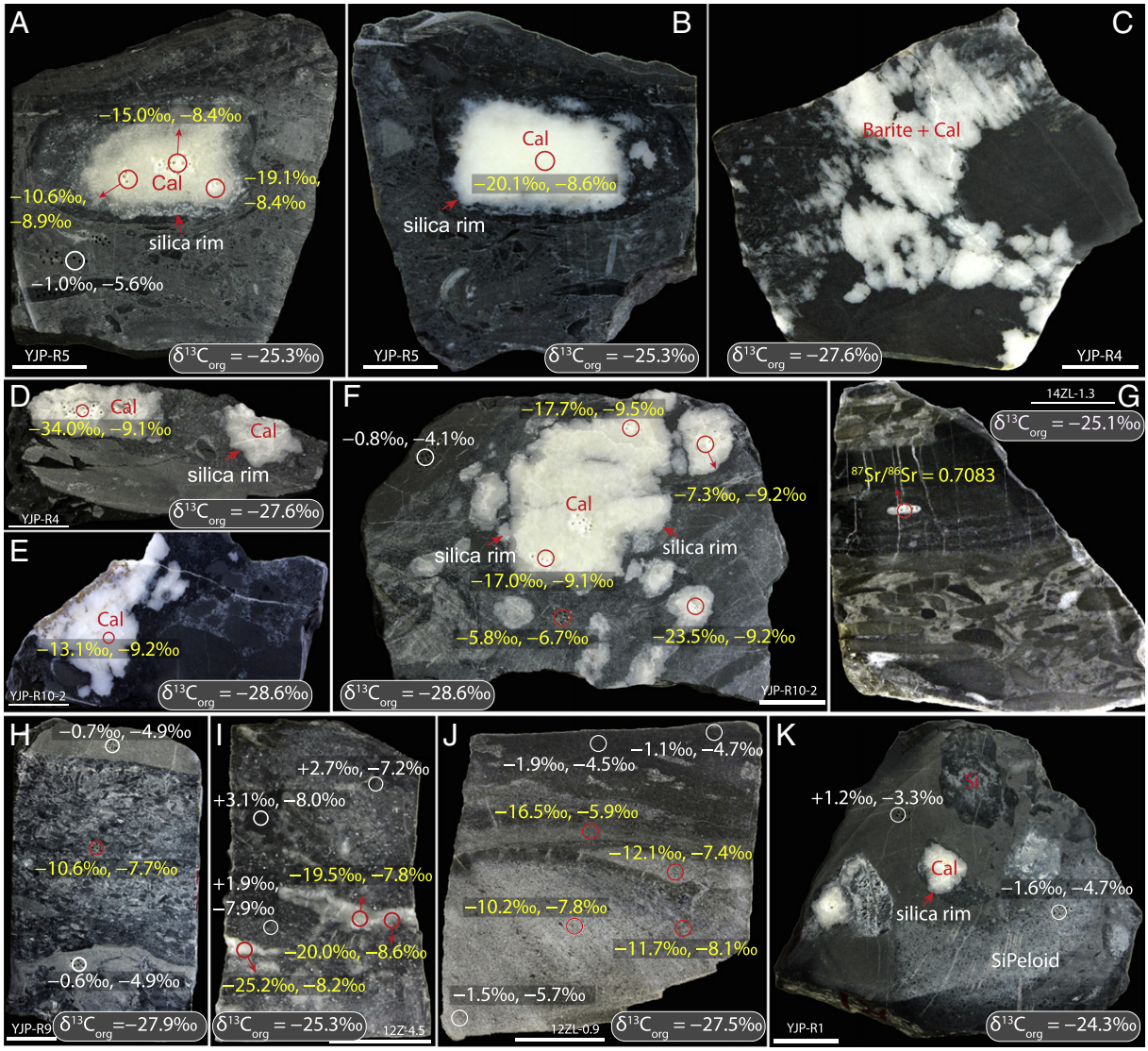

Fig. 4. Geochemical data of phosphorite samples collected from the uppermost Doushantuo Formation at Yangjiaping and Zhongling. All the scale bars are 2 cm in length. Sample numbers are given above scale bars. Paired numbers show $\delta^{13}C_{carb}$ (left) and $\delta^{18}O_{carb}$ values (right). $^{87}Sr/^{86}Sr$ ratios and $\delta^{13}C_{org}$ values are also shown when available. All geochemical measurements were made on micro-drilled powders, except $\delta^{13}C_{org}$ values which were measured from acidified residuals of bulk samples. For paired $\delta^{13}C_{carb}$ and $\delta^{18}O_{carb}$ values, authigenic carbonate signatures are marked in yellow color, while primary carbonate signatures are marked in white color.

additionally measured the strontium isotope composition ($^{87}Sr/^{86}Sr$) of one authigenic calcite nodule in phosphorite sample (14ZL-1.3) collected in the uppermost Doushantuo Formation in Zhongling section and obtained a value of 0.7083 (Fig. 4G), which is notably consistent with the contemporaneous Ediacaran seawater values ranging from 0.7080 to 0.7090 (Melezhik et al., 2009; Sawaki et al., 2010; Cui et al., 2015; Xiao et al., in press).

6. Discussion

6.1. Authigenic origin for the ^{13}C-depleted calcite

To form carbonates with $\delta^{13}C_{carb}$ value less than −30‰, the precipitation fluids normally require a methane source either from biogenic methane through methanogenesis (e.g., Xu, 2010; Drake et al., 2015; Sela-Adler et al., 2015), or thermogenic methane from hydrothermal fluids (e.g., Bristow et al., 2011). In the case of the Doushantuo phosphorites, multiple lines of evidence suggest that the negative $\delta^{13}C_{carb}$ compositions measured from calcite nodules in phosphorite samples are methane-derived authigenic phases formed during very early diagenesis, rather than a late hydrothermal origin. (1) $^{87}Sr/^{86}Sr$ of calcite nodules reveal typical Ediacaran seawater value around 0.7083 (Fig. 4H), suggesting authigenic calcite mineralization in shallow marine sediments that were in free exchange with ambient seawater, and were not influenced by hydrothermal fluids (*cf.* Bristow et al., 2011). The observation that authigenic carbonates record seawater Sr signals is typical of Modern marine sediments (e.g., Hovland et al., 1987; Aharon et al., 1997; Naehr et al., 2000; Greinert et al., 2001; Peckmann et al., 2001; Joseph et al., 2012). If the marine sediments are unconsolidated with free diffusion of Sr from seawater, authigenic carbonate nodules and cements would capture seawater Sr isotope compositions. (2) All authigenic calcites are preserved three-dimensionally as nodules inside the phosphorite host rock (Figs. 3, 4), and they are not directly associated with hydrothermal veins. (3) All the authigenic calcite nodules are surrounded by an authigenic silica or barite rim growing centripetally towards the calcite nodule (Fig. 3 G–J), suggesting that the rim was formed before or simultaneously with the calcite during dissolution of preexisting sediments. Such texture could not be reconciled by the interpretation of a simple hydrothermal pulse. (4) CL images of authigenic calcite nodules show dim

Table 1
Geochemical data analyzed from the phosphorite samples in the uppermost Doushantuo Formation at Yangjiaping and Zhongling.

Sample	Calcite nodules		Phosphorite or phosphatic dolostone matrix		Bulk acidified residuals
	$\delta^{13}C_{carb}$ (‰, PDB)	$\delta^{18}O_{carb}$ (‰, PDB)	$\delta^{13}C_{carb}$ (‰, PDB)	$\delta^{18}O_{carb}$ (‰, PDB)	$\delta^{13}C_{org}$ (‰, PDB)
YJP–R5	−15.0	−8.4	−1.0	−5.6	−25.3
(Yangjiaping)	−19.1	−8.4			
	−10.6	−8.9			
	−20.1	−8.6			
YJP–R4	−34.0	−9.1			−27.6
(Yangjiaping)					
YJP–R10–2	−17.7	−9.5	−0.8	−4.1	
(Yangjiaping)	−7.3	−9.2			
	−17.0	−9.1			−28.6
	−5.8	−6.7			
	−23.5	−9.2			
	−13.1	−9.2			
YJP–R9	−10.6	−7.7	−0.6	−4.9	−27.9
(Yangjiaping)			−0.7	−4.9	
YJP–R1			−1.6	−4.7	−24.3
(Yangjiaping)			+1.2	−3.3	
12Z–4.5	−19.5	−7.8	+2.7	−7.2	−25.3
(Zhongling)	−20.0	−8.6	+3.1	−8.0	
	−25.2	−8.2	+1.9	−7.9	
12Z–0.9	−11.7	−8.1	−1.5	−5.7	−27.5
(Zhongling)	−12.1	−7.4	−1.1	−4.7	
	−16.5	−5.9	−1.9	−4.5	
	−10.2	−7.8			

color, indicating a primary seawater signal with a low Mn/Fe ratio, rather than late diagenetic alteration (Fig. 3M). Bright orange luminescence under CL was indeed observed, but is only limited to dolomitized cements between granular phosphorite (Fig. 3N, O). Thus, based on these petrographic observations and geochemical data, we conclude that the $\delta^{13}C_{carb}$ data largely reflect primary low-temperature signals during deposition and authigenesis.

6.2. Redox conditions during phosphogenesis

Based on an integrated basin-scale chemostratigraphic correlation of the Doushantuo Formation, it has been proposed that both the inner shelf and outer shelf sections are stratigraphically incomplete, and phosphorite horizons in the uppermost outer shelf Zhongling and Yangjiaping sections were at least partly correlated with the EN3a interval of the intra-shelf Jiulongwan section (Xiao et al., 2012; Cui et al., 2015) (Fig. 5). In contrast, a recent study correlated the uppermost Doushantuo Formation in the outer shelf sections with the middle-Doushantuo EN2 interval at Jiulongwan (Furuyama et al., 2016). The main evidence that led to such a correlation is a putative rise in $^{87}Sr/^{86}Sr$ in the EN2 interval at that locality. However, it should be noted that this $^{87}Sr/^{86}Sr$ rise was based on measurements from muddy and silty dolostone with Mn/Sr > 1 and carbonate percentage < 60% (Sawaki et al., 2010). As such, radiogenic Sr from the decay of ^{87}Rb in clays and other silicate minerals may have altered the $^{87}Sr/^{86}Sr$ ratios, and the Furuyama et al.'s (2016) correlation is therefore problematic.

Isotopic data from the uppermost Doushantuo phosphorite interval at the Zhongling and Yangjiaping sections show a decreasing $\delta^{13}C_{carb}$ trend (= decreasing leg of the Shuram Excursion or EN3a interval in Jiulongwan), whereas $^{87}Sr/^{86}Sr$ ratios measured from limestone samples at these two sections reveal a coincident increase to ca. 0.7085, suggesting a carbon cycle fluctuation was triggered by enhanced chemical weathering (Cui et al., 2015). The lack of a complete stratigraphic expression of the Shuram Excurison (characterized by nadir $\delta^{13}C_{carb}$ values of ca. −10‰, or a corresponding rise in $^{87}Sr/^{86}Sr$ ratios up to 0.7090) in outer shelf sections (Fig. 5) might be due to either stratigraphic truncations or a diachronous nature of the Doushantuo/Dengying boundary (Cui et al., 2015).

Based on Ce/Ce* data measured from carbonate and phosphorite samples prepared using dilute acid (0.4 M HNO_3), it was proposed that the upper Zhongling and Yangjiaping sections recorded a redox transition from oxic to reducing environments (Cui et al., 2015). This interpretation is seemingly inconsistent with the abundance of intraclasts and ooids in the phosphatic interval, which indicates an oxygenated shallow shelf depositional environment. This apparent discrepancy can be reconciled by a distinction between redox conditions in surface seawaters vs. bottom seawater or pore waters. Although the depositional environment in the water column was likely to be oxidized, the authigenic environment at the seafloor or in pore waters may be anoxic due to aerobic remineralization of abundant organic matter formed by water column photosynthesis. Multiple lines of evidence suggest that the upper Doushantuo Formation was deposited during a period with enhanced chemical weathering and enlarged sulfate pool (Fike et al., 2006; Kaufman et al., 2007; McFadden et al., 2008; Cui et al., 2015). It is likely that such conditions stimulated strong oceanic redox stratification and deep water anoxia (e.g., Jiang et al., 2007; Ader et al., 2009; Li et al., 2010, 2015; Och et al., 2016; Cui et al., in press; Sahoo et al., in press). In shallow-water environments, although the water column could be oxic, the authigenic environment in porewaters could be anoxic, which affected the Ce/Ce* ratios.

The interpretation of a basin-scale authigenesis pattern is also consistent with the overall trend of $\delta^{13}C_{carb}$ across the basin (Fig. 5). As authigenesis occurs, a considerable amount of organic matter may have been oxidized by sulfate via microbial sulfate reduction, forming ^{13}C-depleted alkalinity. When the alkalinity in pore water became oversaturated, ^{13}C-depleted authigenic carbonates would precipitate (Higgins et al., 2009; Schrag et al., 2013). Supporting evidence also comes from chemostratigraphic sulfur isotope profiles. Paired sulfur isotopes decrease progressively up section toward the upper Doushantuo Formation (Fig. 5), suggesting a continuing increase in the seawater sulfate reservoir in the Ediacaran ocean (McFadden et al., 2008), likely driven by the elevated oxidation of terrestrial pyrite associated with a middle Ediacaran atmospheric oxygenation event (Kaufman et al., 2007; Shields-Zhou and Och, 2011; Liu et al., 2016). Although phosphorites are not found in the EN3 interval at the Jiulongwan section (see discussion in the next section), the close coupling between phosphorite deposition and the upper Doushantuo $\delta^{13}C_{carb}$ negative excursion (Fig. 5) offers new insights into the origin of the Shuram Excursion: the Shuram Excursion may have resulted from enhanced ^{13}C-depleted authigenic carbonate mineralization fueled by pervasive microbial sulfate and iron reduction in the context of an atmospheric oxygenation event. Further investigations on other equivalent successions of the Shuram Excursion at a global scale are needed to test this hypothesis (e.g., Macdonald et al., 2013; Cui, 2015; Kaufman et al., 2015).

6.3. Biogeochemical model for Ediacaran pohosphogenesis

It has been proposed that phosphorite deposits in the Doushantuo Formation at different localities across the basin show a distinct redox- or depth-dependent distribution (Muscente et al., 2015). In South China, most of the phosphorite deposits are preserved in shallow shelf environments, including the inner shelf Baokang, Zhangcunping, Xiaofenghe sections and outer shelf Zhongling, Yangjiaping, Weng'an sections. On the contrary, relatively deeper sections like the intra-shelf Jiulongwan, and slope sections at Siduping, Taoying and Minle lack significant phosphorite deposits (Jiang et al., 2011; She et al., 2014) (Fig. 6A). It is likely that such a remarkable pattern is largely controlled by redox conditions in the water column (Fig. 6B, C).

In shallower inner or outer shelf regions, where oxic conditions dominate the water column (Fig. 6B), iron oxyhydroxide (FeOOH) efficiently absorbs dissolved phosphate derived from upwelled water masses or riverine input, and then transports the Fe-bound phosphorous

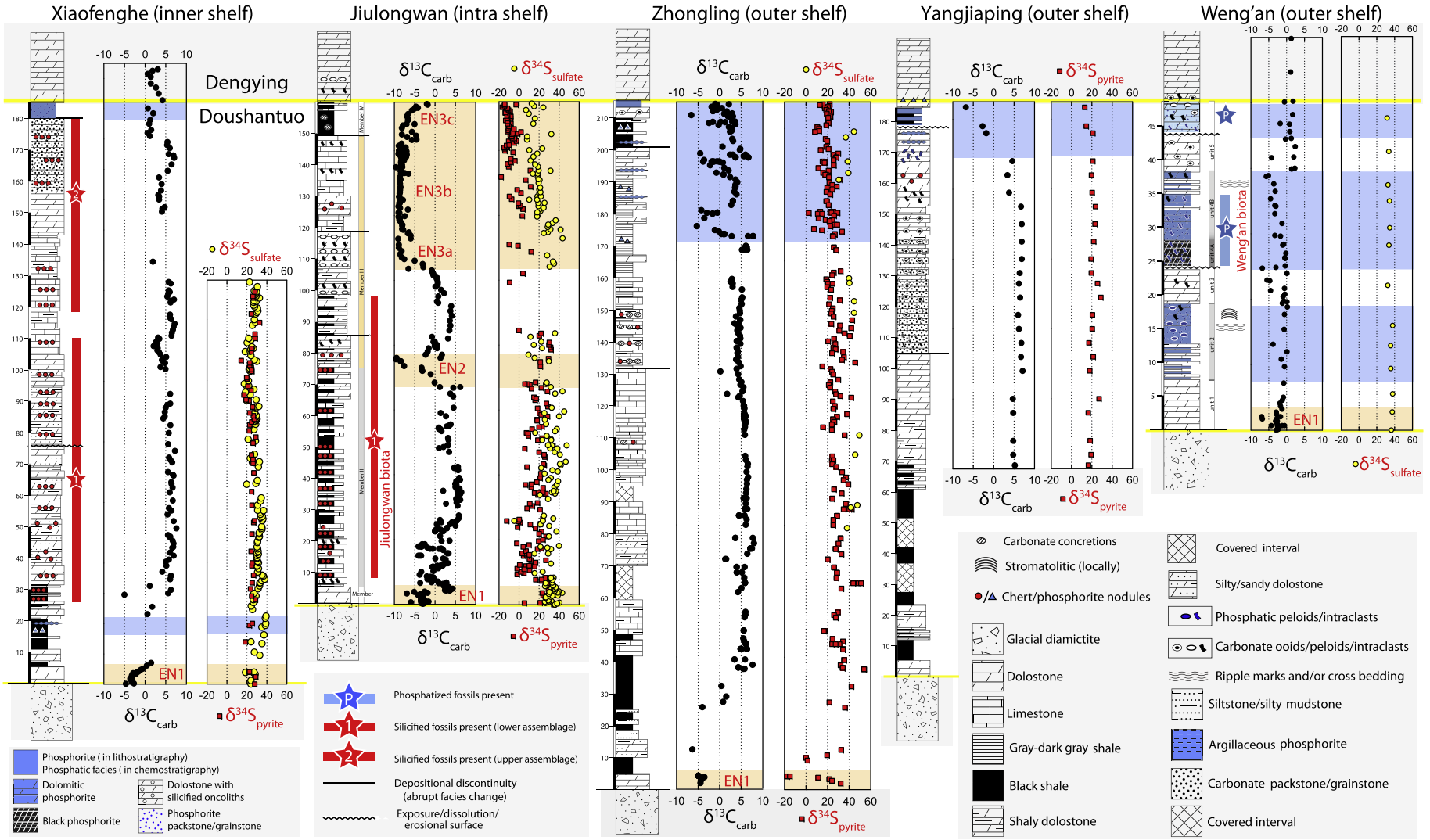

Fig. 5. Integrated litho-, bio-, and chemo-stratigraphy of representative sections of the Doushantuo Formation with phosphorite deposits. The Jiulongwan section, though lacking phosphorite, has also been presented for intra-basinal chemostratigraphic correlation. Lithology columns and fossil assemblages are modified after Jiang et al. (2011) and Muscente et al. (2015). Source of carbon and sulfur isotope data: Xiaofenghe section (Xiao et al., 2012; Zhu et al., 2013), Jiulongwan section (Jiang et al., 2007; McFadden et al., 2008), Zhongling section (Li et al., 2010; Cui et al., 2015), Yangjiaping section (Cui et al., 2015), Weng'an section (Shields et al., 2004; Jiang et al., 2008). Note that $\delta^{34}S_{sulfate}$ data of the Xiaofenghe, Jiulongwan, Zhongling sections are measured from extracted carbonate-associated sulfate (CAS), and $\delta^{34}S_{sulfate}$ data of the Weng'an section are measured from francolite-bound sulphate. Intervals of phosphorite are marked in blue color in the stratocolumn. Ediacaran negative (EN) $\delta^{13}C_{carb}$ excursions as recorded at the Jiulongwan section are marked as EN1, EN2, and EN3 (McFadden et al., 2008).

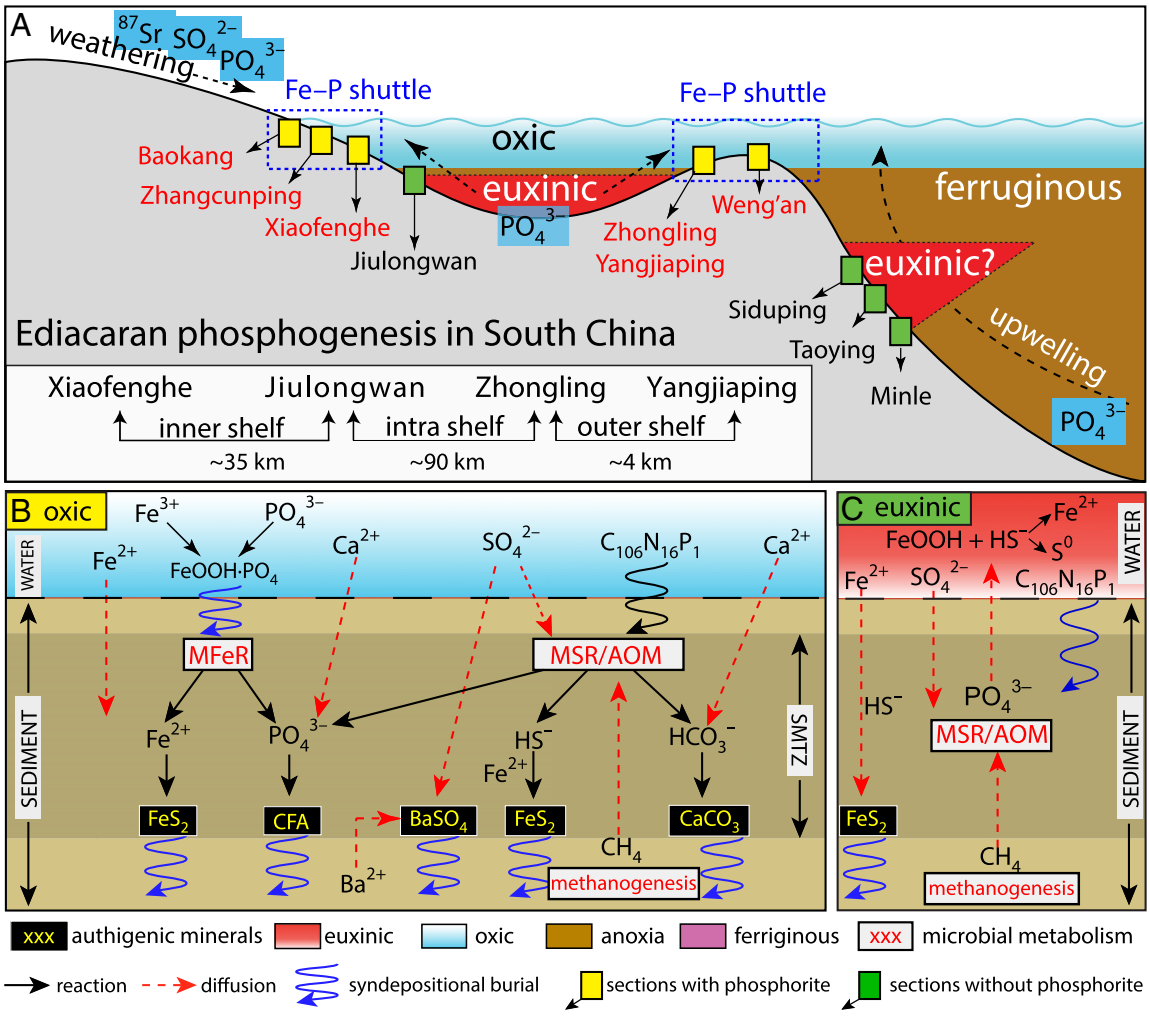

Fig. 6. Biogeochemical model of Ediacaran phosphogenesis in continental margins of South China. **(A)** Simplified basin-scale depositional reconstruction of the Doushantuo Formation (Jiang et al., 2011; Xiao et al., 2012; Cui et al., 2015; Muscente et al., 2015), showing locations of stratigraphic sections mentioned in the text and sources of phosphorus, sulfate, and radiogenic strontium. **(B)** Geomicrobial processes responsible for phosphogenesis in an oxic/suboxic oceanic environment (e.g., inner shelf sections at Baokang, Zhangcunping, and Xiaofenghe; outer shelf sections at Zhongling, Yangjiaping and Weng'an). **(C)** Geomicrobial processes in a euxinic oceanic environment (e.g., intra-shelf section at Jiulongwan and slope section at Siduping, Taoying, and Minle). Modified after Glenn et al. (1994) and Muscente et al. (2015). CFA = carbonate fluorapatite; MSR = microbial sulfate reduction; AOM = anaerobic oxidation of methane; MFeR = Microbial iron reduction; SMTZ = sulfate–methane transition zone. See the main text for detailed discussion.

($FeOOH \cdot PO_4$) into marine sediments (Berner, 1973; Shaffer, 1986; Feely et al., 1991, 1998; Poulton and Canfield, 2006). This "Fe–P shuttle" functions as the main mechanism of phosphorous burial (Glenn et al., 1994; Shen et al., 2000). On the contrary, in euxinic environments where free sulfide is present in the water column (Fig. 6C), iron oxyhydroxides would react with sulfide, forming ferrous iron and elemental sulfur. The scavenging of iron oxyhydroxide by free sulfide shuts down the "Fe–P shuttle", thus dissolved phosphorous is not incorporated into the sediments (März et al., 2008). This model could possibly explain the lack of phosphorite deposits in anoxic or euxinic environments (e.g., the intra-shelf Jiulongwan section and deeper slope/basinal sections) in South China. Anoxic (including euxinic) conditions in bottom water masses, or in a restricted basin, would thus promote the accumulation of dissolved phosphorus near the redox interface, which could be transported into shallow oxidizing environments as a source for phosphorites during upwelling events (Nelson et al., 2010; She et al., 2013, 2014).

Once the absorbed Fe-bound phosphorous ($FeOOH \cdot PO_4$) is transported into the marine sediments, phosphorous is concentrated in the pore water to promote phosphate mineralization (Glenn and Arthur, 1990; Kim et al., 1999). Considering that microbial sulfate reduction is the dominant process in organic C degradation in modern marine sediments (Jørgensen, 1982; Thamdrup and Canfield, 1996; Jørgensen and Kasten, 2006), it is likely to be an important process driving phosphorite formation in the Doushantuo Formation. In light of the abundance of ^{13}C-depleted authigenic carbonate and authigenic calcite, barite, and pyrite in association with Doushantuo phosphorite, microbial sulfate reduction (MSR) likely played an important role in the deposition of Doushantuo phosphorite. Assuming that the phosphatic intraclasts in the Doushantuo Formation were reworked over a short distance soon after their lithification, it is possible that MSR may have facilitated phosphogenesis by concentrating phosphorous in pore waters. During microbial sulfate and iron reduction, phosphorous is released from $FeOOH \cdot PO_4$ or organic matter, the concentration of pore water phosphate is raised above the supersaturation levels, and amorphous phosphate would precipitate (Filippelli, 2001, 2008).

Another line of evidence that supports our view is the abundance of disseminated authigenic pyrite in the studied Doushantuo phosphorite samples (Fig. 2G–L). Enhanced phosphate release into pore water normally occurs in the presence of sulfate, which fuels sulfate reduction, and, as a result, authigenic sulfide minerals would form in the sediments (Roden and Edmonds, 1997; Konhauser et al., 2011a, 2011b). Consistent with what we observed at Yangjiaping and Zhongling, abundant authigenic pyrite is also present in Doushantuo phosphorites at Weng'an (Dornbos et al., 2006), Zhongling (Jiang et al., 2011), Yangjiaping (Cui et al., 2015), and North Xiaofenghe (Xiao et al., 2012), suggesting that

reactive iron and hydrogen sulfide were available in the pore waters, mostly likely derived from microbial sulfate reduction. Although some pyrite grains might have been recrystallized to form larger crystals during later burial, the widespread distribution and high abundance of pyrite in Doushantuo phosphorites supports the view that microbial sulfate reduction played an important role in phosphogenesis.

It should be noted that the phosphorite rocks in the uppermost Doushantuo Formation are mostly intraclastic in texture (Figs. 2, 3). This suggests the occurrence of sediment reworking before final deposition (e.g., She et al., 2013, 2014; Cui et al., 2015; Álvaro et al., 2016). Thus, the ^{13}C-depleted authigenic calcite only records authigenetic history after the final deposition of phosphatic intraclasts. However, because of the consistent stratigraphic and environmental distribution of the upper Doushantuo phosphorite, it is likely that the intraclasts were phosphotized early and soon transported to where they were cemented. Thus, the close coupling between phosphorite and isotopically-distinct authigenic minerals and phosphorites still offers useful insights on the carbon, phosphorite cycling and phosphorite formation during the Ediacaran Period. Taken together, microbially mediated sulfate reduction, the degradation of organic matter, methanogenesis, anaerobic oxidation of methane, and Fe recycling during early diagenesis may have played an important role in concentrating phosphorous within pore water, facilitating phosphorite precipitation in the Ediacaran Period (Fig. 6).

6.4. Phosphorous cycling and the Neoproterozoic Oxygenation Event

Phosphorous has been argued to be a critical factor to maintain the widespread ferruginous condition in the ocean before the Ediacaran Period (Bjerrum and Canfield, 2002; Poulton and Canfield, 2011). It has been suggested that low phosphorus availability may have significantly reduced the rates of photosynthesis and organic carbon burial, thereby resulting in a long-term delay in the rise of atmospheric oxygen rise during the late Archaean and early Proterozoic (Bjerrum and Canfield, 2002).

In contrast to the general absence of phosphorites in early Earth's history, widespread phosphogenesis during the Ediacaran Period stands out, and is likely coupled with profound changes in atmospheric oxygenation, as well as the evolution of seawater redox conditions (Cook and Shergold, 1984; Brasier, 1992; Cook, 1992; Papineau, 2010; Planavsky et al., 2010). Coincident with the Ediacaran phosphogenic event, an increase of seawater $^{87}Sr/^{86}Sr$ during the late Ediacaran suggests enhanced chemical weathering and terrestrial input of sulfate into the middle Ediacaran ocean (Kaufman et al., 1993; Halverson et al., 2007; Cui et al., 2015). Such enhancement in chemical weathering is probably a result of active tectonic uplift during Pan-African assembly (Kaufman et al., 1993; Li, 2011; Li et al., 2013). Consistent with enhanced chemical weathering, an increased flux of phosphorous into the Ediacaran ocean may have promoted primary productivity and organic carbon burial, causing a net increase of atmospheric O_2 (Campbell and Allen, 2008; Campbell and Squire, 2010; Planavsky et al., 2010) (Fig. 7). Enhanced primary productivity may also increase the oxygen consumption in the water columns, which would drive the expansion of the oxygen minimum zone (OMZ) and potentially cause an ocean anoxia event (Cui et al., in press; Sahoo et al., in press).

Perturbations in ocean redox conditions are believed to have a significant impact on marine phosphorous cycling. A comprehensive investigation (Colman and Holland, 2000) on the diffusive return flux of phosphate from marine sediments beneath both oxic and anoxic water columns reveals a strong coupling between the redox state of marine sediments and the return flux of phosphate to seawater. The flux of phosphate in highly reduced sediments is significantly higher than that from highly oxidized sediments. If correct, this suggests that the marine phosphate cycle is critically linked to oceanic redox conditions and the stabilization of atmospheric oxygen.

During ocean anoxia, more dissolved phosphorous derived from organic C degradation would be recycled into the shallow ocean through upwelling, and stimulate greater primary productivity, which would further cause an even stronger biological pump, developing a *positive* feedback loop of "primary productivity → ocean anoxia → phosphorous recycling → more primary productivity → more ocean anoxia" (Van Cappellen and Ingall, 1994, 1996; Mort et al., 2007) (Fig. 7). However, this positive feedback could also operate in the opposite direction. When larger and more complex eukaryotic particles emerged and sank more rapidly through the water column, oxygen demand could shift away from the surface, leading to the expansion of mid-depth oxygenation, enhanced removal of phosphorus, a reduce in primary productivity and oxygen demand, and further expansion of oxygenation (Butterfield, 2009, 2011; Lenton et al., 2014; Butterfield, 2015).

Alternatively, a *negative* feedback on carbon and phosphorous cycling may have played a role on stabilizing the oxygen concentrations in the Early Cambrian (Boyle et al., 2014). As bioturbation evolved, the retention of phosphorous (relative to carbon) within organic matter in

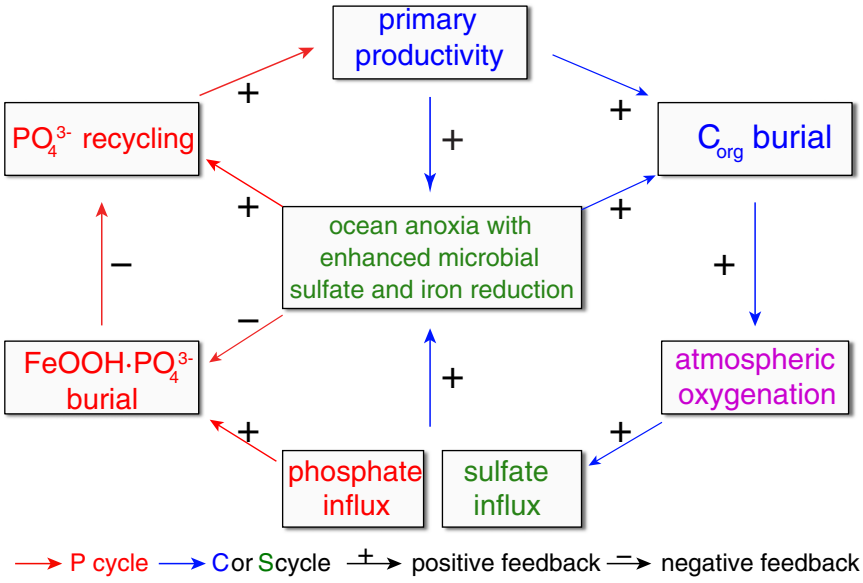

Fig. 7. Biogeochemical feedbacks of carbon, sulfur and phosphorous cycling during the Ediacaran Period. See the main text for detailed discussion.

marine sediments should have been enhanced, thereby a negative feedback loop of "more bioturbation → increase in phosphorous burial and decrease in global oxygen reservoir → limited bioturbation" may be initiated. However, this negative feedback is more effective in the Phanerozoic, particularly when vertical bioturbation became more intense after the late Silurian, 120 million years after the Precambrian–Cambrian transition (Tarhan and Droser, 2014; Tarhan et al., 2015).

In summary, biogeochemical carbon, sulfur and phosphorous cycling in the Ediacaran Period show strong coupling along with the oxygenation of the atmosphere and hydrosphere, which may have had a profound impact on early animal evolution and taphonomic preservation. The operation of both positive and negative feedback loops in the biogeochemical C–P cycling played a critical role in balancing the evolutionary trajectory of Earth's redox condition.

7. Conclusions

Detailed sedimentological and geochemical investigations have been conducted on the Ediacaran phosphorite samples collected from the upper Doushantuo Formation in South China. The discovery of authigenic calcite, barite, and pyrite in the studied samples, coupled with profound ^{13}C-depletion in authigenic calcite cements and nodules, suggests that middle Ediacaran phosphogenesis was driven by microbial sulfate and iron reduction in marine sediments, which may have enriched the phosphorous concentration in pore waters, thus facilitating the formation of phosphorite. Our study provides important evidence for an authigenic origin of middle Ediacaran phosphorites, and suggests that this local phosphogenic event was closely linked to the greatest negative carbon cycle anomaly (i.e., the Shuram Excursion), and may be found in similarly aged sedimentary successions around the world.

Acknowledgements

We thank Mike Evans and Zhengting Wang for their assistance in the UMD Paleoclimate Co-Laboratory, and Timothy Rose for the guidance on using the Cathodoluminescence Microscope and Spectrometer in the Department of Mineral Sciences, Smithsonian Institution, Washington, DC. We also thank Drew Muscente, Xiao-Ming Liu and Zhenbing She for helpful comments. This research is supported by grants from the NASA Exobiology (NNX12AR91G to AJK and NNX15AL27G to SX), the NSF Sedimentary Geology and Paleontology program (EAR-0844270 to AJK and EAR-1528553 to SX), the Society of Economic Geologists Student Research Grant (to HC), the Explorers Club Exploration Fund Grant (to HC), and the American Association of Petroleum Geologists Grants-In-Aid Program (to HC). HC also thanks the NASA Astrobiology Institute in the University of Wisconsin-Madison for support. The manuscript benefits from constructive reviews by James Schiffbauer and an anonymous reviewer.

References

Ader, M., Macouin, M., Trindade, R.I.F., Hadrien, M.H., Yang, Z., Sun, Z., Besse, J., 2009. A multilayered water column in the Ediacaran Yangtze platform? Insights from carbonate and organic matter paired $\delta^{13}C$. Earth and Planetary Science Letters 288, 213–227.

Aharon, P., Schwarcz, H.P., Roberts, H.H., 1997. Radiometric dating of submarine hydrocarbon seeps in the Gulf of Mexico. Geological Society of America Bulletin 109, 568–579.

Álvaro, J.J., Shields-Zhou, G.A., Ahlberg, P., Jensen, S., Palacios, T., 2016. Ediacaran–Cambrian phosphorites from the western margins of Gondwana and Baltica. Sedimentology 63, 350–377.

An, Z., Jiang, G., Tong, J., Tian, L., Ye, Q., Song, H., Song, H., 2015. Stratigraphic position of the Ediacaran Miaohe biota and its constrains on the age of the upper Doushantuo $\delta^{13}C$ anomaly in the Yangtze Gorges area, South China. Precambrian Research 271, 243–253.

Arning, E., Birgel, D., Brunner, B., Peckmann, J., 2009. Bacterial formation of phosphatic laminites off Peru. Geobiology 7, 295–307.

Berner, R.A., 1973. Phosphate removal from sea water by adsorption on volcanogenic ferric oxides. Earth and Planetary Science Letters 18, 77–86.

Bjerrum, C.J., Canfield, D.E., 2002. Ocean productivity before about 1.9 Gyr ago limited by phosphorus adsorption onto iron oxides. Nature 417, 159–162.

Boyle, R.A., Dahl, T.W., Dale, A.W., Shields-Zhou, G.A., Zhu, M., Brasier, M.D., Canfield, D.E., Lenton, T.M., 2014. Stabilization of the coupled oxygen and phosphorus cycles by the evolution of bioturbation. Nature Geoscience 7, 671–676.

Brasier, M.D., 1992. Paleoceanography and changes in the biological cycling of phosphorus across the Precambrian–Cambrian boundary. In: Lipps, J.H., Signor, P.W. (Eds.), Origin and Early Evolution of the Metazoa. Springer Science & Business Media, New York, USA, pp. 483–523.

Bristow, T.F., Bonifacie, M., Derkowski, A., Eiler, J.M., Grotzinger, J.P., 2011. A hydrothermal origin for isotopically anomalous cap dolostone cements from south China. Nature 474, 68–71.

Butterfield, N.J., 2009. Oxygen, animals and oceanic ventilation: an alternative view. Geobiology 7, 1–7.

Butterfield, N.J., 2011. Animals and the invention of the Phanerozoic Earth system. Trends in Ecology & Evolution 26, 81–87.

Butterfield, N.J., 2015. The Neoproterozoic. Current Biology 25, R859–R863.

Campbell, I.H., Allen, C.M., 2008. Formation of supercontinents linked to increases in atmospheric oxygen. Nature Geoscience 1, 554–558.

Campbell, I.H., Squire, R.J., 2010. The mountains that triggered the Late Neoproterozoic increase in oxygen: The Second Great Oxidation Event. Geochimica et Cosmochimica Acta 74, 4187–4206.

Chen, Z., Zhou, C., Meyer, M., Xiang, K., Schiffbauer, J.D., Yuan, X., Xiao, S., 2013. Trace fossil evidence for Ediacaran bilaterian animals with complex behaviors. Precambrian Research 224, 690–701.

Chen, Z., Zhou, C., Xiao, S., Wang, W., Guan, C., Hua, H., Yuan, X., 2014. New Ediacara fossils preserved in marine limestone and their ecological implications. Scientific Reports 4, 4180.

Colman, A.S., Holland, H.D., 2000. The global diagenetic flux of phosphorus from marine sediments to the oceans: redox sensitivity and the control of atmospheric oxygen levels. In: Glenn, C.R., Prevot-Lucas, L., Lucas, J. (Eds.), Marine Authigenesis: From Global to Microbial. SEPM Special Publication No. 66. Society for Sedimentary Geology (SEPM), Tullsa, Oklahoma, U.S.A., pp. 53–75.

Condon, D., Zhu, M., Bowring, S., Wang, W., Yang, A., Jin, Y., 2005. U–Pb ages from the Neoproterozoic Doushantuo Formation, China. Science 308, 95–98.

Cook, P.J., 1992. Phosphogenesis around the Proterozoic–Phanerozoic transition. Journal of the Geological Society 149, 615–620.

Cook, P.J., Shergold, J.H., 1984. Phosphorus, phosphorites and skeletal evolution at the Precambrian–Cambrian boundary. Nature 308, 231–236.

Creveling, J.R., Knoll, A.H., Johnston, D.T., 2014. Taphonomy of cambrian phosphatic small shelly fossils. PALAIOS 29, 295–308.

Cui, H., 2015. Authigenesis, Biomineralization, and Carbon–Sulfur Cycling in the Ediacaran Ocean (Ph.D. dissertation) University of Maryland, College Park.

Cui, H., Kaufman, A.J., Xiao, S., Peek, S., Cao, H., Min, X., Cai, Y., Siegel, Z., Liu, X.M., Peng, Y., Schiffbauer, J.D., Martin, A.J., 2016. Environmental context for the terminal Ediacaran biomineralization of animals. Geobiology http://dx.doi.org/10.1111/gbi.12178 (in press).

Cui, H., Kaufman, A.J., Xiao, S., Zhu, M., Zhou, C., Liu, X.-M., 2015. Redox architecture of an Ediacaran ocean margin: integrated chemostratigraphic ($\delta^{13}C$–$\delta^{34}S$–$^{87}Sr/^{86}Sr$–Ce/Ce*) correlation of the Doushantuo Formation, South China. Chemical Geology 405, 48–62.

Diaz, J., Ingall, E., Benitez-Nelson, C., Paterson, D., de Jonge, M.D., McNulty, I., Brandes, J.A., 2008. Marine polyphosphate: a key player in geologic phosphorus sequestration. Science 320, 652–655.

Dong, X.-P., Cunningham, J.A., Bengtson, S., Thomas, C.-W., Liu, J., Stampanoni, M., Donoghue, P.C.J., 2013. Embryos, polyps and medusae of the Early Cambrian scyphozoan *Olivooides*. Proceedings of the Royal Society of London B: Biological Sciences 280, 20130071.

Dong, X.-P., Donoghue, P.C., Cheng, H., Liu, J.-B., 2004. Fossil embryos from the Middle and Late Cambrian period of Hunan, south China. Nature 427, 237–240.

Dornbos, S.Q., Bottjer, D.J., Chen, J.-Y., Gao, F., Oliveri, P., Li, C.-W., 2006. Environmental controls on the taphonomy of phosphatized animals and animal embryos from the Neoproterozoic Doushantuo Formation, southwest China. PALAIOS 21, 3–14.

Drake, H., Astrom, M.E., Heim, C., Broman, C., Astrom, J., Whitehouse, M., Ivarsson, M., Siljestrom, S., Sjovall, P., 2015. Extreme ^{13}C depletion of carbonates formed during oxidation of biogenic methane in fractured granite. Nature Communications 6, 7020.

Duda, J.-P., Zhu, M., Reitner, J., 2015. Depositional dynamics of a bituminous carbonate facies in a tectonically induced intra-platform basin: the Shibantan Member (Dengying Formation, Ediacaran Period). Carbonates and Evaporites 31, 87–99.

Dzik, J., 1994. Evolution of 'small shelly fossils' assemblages of the Early Paleozoic. Acta Palaeontologica Polonica 39, 247–313.

Feely, R.A., Trefry, J.H., Lebon, G.T., German, C.R., 1998. The relationship between P/Fe and V/Fe ratios in hydrothermal precipitates and dissolved phosphate in seawater. Geophysical Research Letters 25, 2253–2256.

Feely, R.A., Trefry, J.H., Massoth, G.J., Metz, S., 1991. A comparison of the scavenging of phosphorus and arsenic from seawater by hydrothermal iron oxyhydroxides in the Atlantic and Pacific Oceans. Deep Sea Research 38, 617–623.

Fike, D.A., Grotzinger, J.P., Pratt, L.M., Summons, R.E., 2006. Oxidation of the Ediacaran ocean. Nature 444, 744–747.

Filippelli, G.M., 2001. Carbon and phosphorus cycling in anoxic sediments of the Saanich Inlet, British Columbia. Marine Geology 174, 307–321.

Filippelli, G.M., 2008. The global phosphorus cycle: past, present, and future. Elements 4, 89–95.

Furuyama, S., Kano, A., Kunimitsu, Y., Ishikawa, T., Wei, W., 2016. Diagenetic overprint to a negative carbon isotope anomaly associated with the Gaskiers glaciation of the Ediacaran Doushantuo Formation in South China. Precambrian Research 110–122.

Glenn, C.R., Arthur, M.A., 1990. Anatomy and origin of a Cretaceous phosphorite-greensand giant, Egypt. Sedimentology 37, 123–154.
Glenn, C.R., Föllmi, K.B., Riggs, S.R., Baturin, G.N., Grimm, K.A., Trappe, J., Abed, A.M., Galli-Oliver, C., Garrison, R.E., Ilyan, A., Jehl, C., Rohrlich, V., Sadaqah, R.M., Schidlowski, M., Sheldon, R.E., Siegmund, H., 1994. Phosphorus and phosphorites: sedimentology and environments of formation. Eclogae Geologicae Helvetiae 87, 747–788.
Greinert, J., Bohrmann, G., Suess, E., 2001. Gas hydrate-associated carbonates and methane-venting at Hydrate Ridge: classification, distribution, and origin of authigenic lithologies. In: Paull, C.K., Dillon, W.P. (Eds.), Natural Gas Hydrates: Occurrence, Distribution, and Detection. American Geophysical Union, Washington, D. C., pp. 99–113.
Halverson, G.P., Dudás, F.Ö., Maloof, A.C., Bowring, S.A., 2007. Evolution of the $^{87}Sr/^{86}Sr$ composition of Neoproterozoic seawater. Palaeogeography, Palaeoclimatology, Palaeoecology 256, 103–129.
Higgins, J., Fischer, W., Schrag, D., 2009. Oxygenation of the ocean and sediments: consequences for the seafloor carbonate factory. Earth and Planetary Science Letters 284, 25–33.
Hovland, M., Talbot, M.R., Qvale, H., Olaussen, S., Aasberg, L., 1987. Methane-related carbonate cements in pockmarks of the North Sea. Journal of Sedimentary Research 57, 881–892.
Jiang, G., Kaufman, A.J., Christie-Blick, N., Zhang, S., Wu, H., 2007. Carbon isotope variability across the Ediacaran Yangtze platform in South China: implications for a large surface-to-deep ocean $\delta^{13}C$ gradient. Earth and Planetary Science Letters 261, 303–320.
Jiang, G., Shi, X., Zhang, S., Wang, Y., Xiao, S., 2011. Stratigraphy and paleogeography of the Ediacaran Doushantuo Formation (ca. 635–551 Ma) in South China. Gondwana Research 19, 831–849.
Jiang, G., Zhang, S., Shi, X., Wang, X., 2008. Chemocline instability and isotope variations of the Ediacaran Doushantuo basin in South China. Science in China Series D: Earth Sciences 51, 1560–1569.
Jørgensen, B.B., 1982. Mineralization of organic matter in the sea bed—the role of sulphate reduction. Nature 296, 643–645.
Jørgensen, B.B., Kasten, S., 2006. Sulfur cycling and methane oxidation. In: Schulz, H.D., Zabel, M. (Eds.), Marine Geochemistry. Springer-Verlag, Berlin Heidelberg, Berlin, pp. 271–309.
Joseph, C., Torres, M., Martin, R., Haley, B., Pohlman, J., Riedel, M., Rose, K., 2012. Using the $^{87}Sr/^{86}Sr$ of modern and paleoseep carbonates from northern Cascadia to link modern fluid flow to the past. Chemical Geology 334, 122–130.
Kaufman, A.J., Corsetti, F.A., Varni, M.A., 2007. The effect of rising atmospheric oxygen on carbon and sulfur isotope anomalies in the Neoproterozoic Johnnie Formation, Death Valley, USA. Chemical Geology 237, 47–63.
Kaufman, A.J., Jacobsen, S.B., Knoll, A.H., 1993. The Vendian record of Sr and C isotopic variations in seawater: implications for tectonics and paleoclimate. Earth and Planetary Science Letters 120, 409–430.
Kaufman, A.J., Kriesfeld, L., Cui, H., Narbonne, G.M., Vickers-Rich, P., Zhou, C., Xiao, S., 2015. An authigenic origin for the middle Ediacaran Shuram excursion: the view from Namibia and South China. 2015 GSA Annual Meeting. The Geological Society of America, Baltimore, Maryland, USA.
Kim, D., Schuffert, J.D., Kastner, M., 1999. Francolite authigenesis in California continental slope sediments and its implications for the marine P cycle. Geochimica et Cosmochimica Acta 63, 3477–3485.
Konhauser, K.O., Gingras, M., Kappler, A., 2011a. Sediment diagenesis—biologically controlled. In: Reitner, J., Thiel, V. (Eds.), Encyclopedia of GeobiologyEncyclopedia of Earth Sciences Series. Springer, Netherlands, pp. 777–784.
Konhauser, K.O., Kappler, A., Roden, E.E., 2011b. Iron in microbial metabolisms. Elements 7, 89–93.
Kunimitsu, Y., Setsuda, Y., Furuyama, S., Wang, W., Kano, A., 2011. Ediacaran chemostratigraphy and paleoceanography at a shallow marine setting in northwestern Hunan Province, South China. Precambrian Research 191, 194–208.
Lenton, T.M., Boyle, R.A., Poulton, S.W., Shields-Zhou, G.A., Butterfield, N.J., 2014. Co-evolution of eukaryotes and ocean oxygenation in the Neoproterozoic era. Nature Geoscience 7, 257–265.
Li, Y., 1986. Proterozoic and Cambrian Phosphorites—Regional Review: China, Phosphate Deposits of the World. Proterozoic and Cambrian Phosphorites vol. 1 pp. 42–62.
Li, Z.-X., 2011. Breakup of Rodinia. In: Reitner, J., Thiel, V. (Eds.), Encyclopedia of GeobiologyEncyclopedia of Earth Sciences Series. Springer, Netherlands, pp. 206–210.
Li, C., Cheng, M., Algeo, T., Xie, S., 2015. A theoretical prediction of chemical zonation in early oceans (>520 Ma). Science China: Earth Sciences 11, 1901–1909.
Li, Z.-X., Evans, D.A.D., Halverson, G.P., 2013. Neoproterozoic glaciations in a revised global palaeogeography from the breakup of Rodinia to the assembly of Gondwanaland. Sedimentary Geology 294, 219–232.
Li, C., Love, G.D., Lyons, T.W., Fike, D.A., Sessions, A.L., Chu, X., 2010. A stratified redox model for the Ediacaran ocean. Science 328, 80–83.
Liu, Y., Xiao, S., Shao, T., Broce, J., Zhang, H., 2014b. The oldest known priapulid-like scalidophoran animal and its implications for the early evolution of cycloneuralians and ecdysozoans. Evolution & Development 16, 155–165.
Liu, P., Xiao, S., Yin, C., Chen, S., Zhou, C., Li, M., 2014a. Ediacaran acanthomorphic acritarchs and other microfossils from chert nodules of the upper Doushantuo Formation in the Yangtze Gorges area, South China. Journal of Paleontology 88, 1–139.
Liu, X.-M., Kah, L.C., Knoll, A.H., Cui, H., Kaufman, A.J., Shahar, A., Hazen, R.M., 2016. Tracing Earth's O_2 evolution using Zn/Fe ratios in marine carbonates. Geochemical Perspectives Letters 2, 24–34.
Macdonald, F.A., Strauss, J.V., Sperling, E.A., Halverson, G.P., Narbonne, G.M., Johnston, D.T., Kunzmann, M., Schrag, D.P., Higgins, J.A., 2013. The stratigraphic relationship between the Shuram carbon isotope excursion, the oxygenation of Neoproterozoic oceans, and the first appearance of the Ediacara biota and bilaterian trace fossils in northwestern Canada. Chemical Geology 362, 250–272.
Martill, D.M., Wilby, P.R., 1994. Lithified prokaryotes associated with fossil soft tissues from the Santana Formation (Cretaceous) of Brazil. Kaupia: Darmstadter Beitrage zur Naturgeschichte 4, 71–77.
März, C., Poulton, S., Beckmann, B., Küster, K., Wagner, T., Kasten, S., 2008. Redox sensitivity of P cycling during marine black shale formation: dynamics of sulfidic and anoxic, non-sulfidic bottom waters. Geochimica et Cosmochimica Acta 72, 3703–3717.
McFadden, K.A., Huang, J., Chu, X., Jiang, G., Kaufman, A.J., Zhou, C., Yuan, X., Xiao, S., 2008. Pulsed oxidation and biological evolution in the Ediacaran Doushantuo Formation. Proceedings of the National Academy of Sciences 105, 3197–3202.
Melezhik, V.A., Pokrovsky, B.G., Fallick, A.E., Kuznetsov, A.B., Bujakaite, M.I., 2009. Constraints on $^{87}Sr/^{86}Sr$ of Late Ediacaran seawater: insight from Siberian high-Sr limestones. Journal of the Geological Society 166, 183–191.
Meyer, M., Xiao, S., Gill, B.C., Schiffbauer, J.D., Chen, Z., Zhou, C., Yuan, X., 2014. Interactions between Ediacaran animals and microbial mats: insights from Lamonte trevallis, a new trace fossil from the Dengying Formation of South China. Palaeogeography, Palaeoclimatology, Palaeoecology 396, 62–74.
Mort, H.P., Adatte, T., Föllmi, K.B., Keller, G., Steinmann, P., Matera, V., Berner, Z., Stüben, D., 2007. Phosphorus and the roles of productivity and nutrient recycling during oceanic anoxic event 2. Geology 35, 483–486.
Muscente, A.D., Hawkins, A.D., Xiao, S., 2015. Fossil preservation through phosphatization and silicification in the Ediacaran Doushantuo Formation (South China): a comparative synthesis. Palaeogeography, Palaeoclimatology, Palaeoecology 434, 46–62.
Naehr, T.H., Rodriguez, N.M., Bohrmann, G., Paull, C.K., Botz, R., 2000. Methane-derived authigenic carbonates associated with gas hydrate decomposition and fluid venting above the Blake Ridge Diapir. In: Paull, C.K., Matsumoto, R., Wallace, P.J., Dillon, W.P. (Eds.), Proceedings of the Ocean Drilling Program. Scientific Results. Ocean Drilling Program, pp. 285–300.
Nelson, G.J., Pufahl, P.K., Hiatt, E.E., 2010. Paleoceanographic constraints on Precambrian phosphorite accumulation, Baraga Group, Michigan, USA. Sedimentary Geology 226, 9–21.
Och, L.M., Cremonese, L., Shields-Zhou, G.A., Poulton, S.W., Struck, U., Ling, H., Li, D., Chen, X., Manning, C., Thirlwall, M., Strauss, H., Zhu, M., 2016. Palaeoceanographic controls on spatial redox distribution over the Yangtze Platform during the Ediacaran–Cambrian transition. Sedimentology 63, 378–410.
Papineau, D., 2010. Global biogeochemical changes at both ends of the Proterozoic: insights from phosphorites. Astrobiology 10, 165–181.
Paytan, A., McLaughlin, K., 2007. The oceanic phosphorus cycle. Chemical Reviews 107, 563–576.
Peckmann, J., Reimer, A., Luth, U., Luth, C., Hansen, B.T., Heinicke, C., Hoefs, J., Reitner, J., 2001. Methane-derived carbonates and authigenic pyrite from the northwestern Black Sea. Marine Geology 177, 129–150.
Planavsky, N.J., Rouxel, O.J., Bekker, A., Lalonde, S.V., Konhauser, K.O., Reinhard, C.T., Lyons, T.W., 2010. The evolution of the marine phosphate reservoir. Nature 467, 1088–1090.
Porter, S.M., 2004. Closing the phosphatization window: testing for the influence of taphonomic megabias on the pattern of small shelly fossil decline. PALAIOS 19, 178–183.
Poulton, S.W., Canfield, D.E., 2006. Co-diagenesis of iron and phosphorus in hydrothermal sediments from the southern East Pacific Rise: implications for the evaluation of paleoseawater phosphate concentrations. Geochimica et Cosmochimica Acta 70, 5883–5898.
Poulton, S.W., Canfield, D.E., 2011. Ferruginous conditions: a dominant feature of the ocean through Earth's history. Elements 7, 107–112.
Roden, E., Edmonds, J., 1997. Phosphate mobilization in iron-rich anaerobic sediments: microbial Fe (III) oxide reduction versus iron-sulfide formation. Archiv für Hydrobiologie 139, 347–378.
Sahoo, S.K., Planavsky, N.J., Jiang, G., Kendall, B., Owens, J.D., Wang, X., Shi, X., Anbar, A.D., Lyons, T.W., 2016. Oceanic oxygenation events in the anoxic Ediacaran ocean. Geobiology. http://dx.doi.org/10.1111/gbi.12182 (in press).
Saltzman, M.R., 2005. Phosphorus, nitrogen, and the redox evolution of the Paleozoic oceans. Geology 33, 573–576.
Sawaki, Y., Ohno, T., Tahata, M., Komiya, T., Hirata, T., Maruyama, S., Windley, B.F., Han, J., Shu, D., Li, Y., 2010. The Ediacaran radiogenic Sr isotope excursion in the Doushantuo Formation in the Three Gorges area, South China. Precambrian Research 176, 46–64.
Schiffbauer, J.D., Wallace, A.F., Broce, J., Xiao, S., 2014. Exceptional fossil conservation through phosphatization. In: Laflamme, M., Schiffbauer, J.D., Darroch, S.A.F. (Eds.), Reading and Writing of the Fossil Record: Preservational Pathways to Exceptional Fossilization. The Paleontological Society Papers, pp. 59–82.
Schmitz, M.D., 2012. Radiometric ages used in GTS2012. In: Gradstein, F.M., Ogg, J.G., Schmitz, M.D., Ogg, G.M. (Eds.), The Geologic Time Scale. Elsevier, Boston, pp. 1045–1082.
Schrag, D.P., Higgins, J.A., Macdonald, F.A., Johnston, D.T., 2013. Authigenic carbonate and the history of the global carbon cycle. Science 339, 540–543.
Sela-Adler, M., Herut, B., Bar-Or, I., Antler, G., Eliani-Russak, E., Levy, E., Makovsky, Y., Sivan, O., 2015. Geochemical evidence for biogenic methane production and consumption in the shallow sediments of the SE Mediterranean shelf (Israel). Continental Shelf Research 101, 117–124.
Shaffer, G., 1986. Phosphate pumps and shuttles in the Black Sea. Nature 321, 515–517.
She, Z.-B., Strother, P., McMahon, G., Nittler, L.R., Wang, J., Zhang, J., Sang, L., Ma, C., Papineau, D., 2013. Terminal Proterozoic cyanobacterial blooms and phosphogenesis documented by the Doushantuo granular phosphorites I: *in situ* micro-analysis of textures and composition. Precambrian Research 235, 20–35.
She, Z.-B., Strother, P., Papineau, D., 2014. Terminal Proterozoic cyanobacterial blooms and phosphogenesis documented by the Doushantuo granular phosphorites II: microbial diversity and C isotopes. Precambrian Research 251, 62–79.
Shen, Y., Schidlowski, M., Chu, X., 2000. Biogeochemical approach to understanding phosphogenic events of the terminal Proterozoic to Cambrian. Palaeogeography, Palaeoclimatology, Palaeoecology 158, 99–108.

Shields, G., Kimura, H., Yang, J., Gammon, P., 2004. Sulphur isotopic evolution of Neoproterozoic-Cambrian seawater: new francolite-bound sulphate $\delta^{34}S$ data and a critical appraisal of the existing record. Chemical Geology 204, 163–182.
Shields-Zhou, G., Och, L., 2011. The case for a Neoproterozoic oxygenation event: geochemical evidence and biological consequences. GSA Today 21, 4–11.
Tarhan, L.G., Droser, M.L., 2014. Widespread delayed mixing in early to middle Cambrian marine shelfal settings. Palaeogeography, Palaeoclimatology, Palaeoecology 399, 310–322.
Tarhan, L.G., Droser, M.L., Planavsky, N.J., Johnston, D.T., 2015. Protracted development of bioturbation through the early Palaeozoic Era. Nature Geoscience 8, 865–869.
Thamdrup, B., Canfield, D.E., 1996. Pathways of carbon oxidation in continental margin sediments off central Chile. Limnology and Oceanography 41, 1629–1650.
Tyrrell, T., 1999. The relative influences of nitrogen and phosphorus on oceanic primary production. Nature 400, 525–531.
Van Cappellen, P., Ingall, E.D., 1994. Benthic phosphorus regeneration, net primary production, and ocean anoxia: a model of the coupled marine biogeochemical cycles of carbon and phosphorus. Paleoceanography 9, 677–692.
Van Cappellen, P., Ingall, E.D., 1996. Redox stabilization of the atmosphere and oceans by phosphorus-limited marine productivity. Science 271, 493–496.
Xiao, S., Knoll, A.H., 1999. Fossil preservation in the Neoproterozoic Doushantuo phosphorite Lagerstätte, South China. Lethaia 32, 219–238.
Xiao, S., Knoll, A.H., Yuan, X., Pueschel, C.M., 2004. Phosphatized multicellular algae in the Neoproterozoic Doushantuo Formation, China, and the early evolution of florideophyte red algae. American Journal of Botany 91, 214–227.
Xiao, S., McFadden, K.A., Peek, S., Kaufman, A.J., Zhou, C., Jiang, G., Hu, J., 2012. Integrated chemostratigraphy of the Doushantuo Formation at the northern Xiaofenghe section (Yangtze Gorges, South China) and its implication for Ediacaran stratigraphic correlation and ocean redox models. Precambrian Research 192–195, 125–141.
Xiao, S., Muscente, A., Chen, L., Zhou, C., Schiffbauer, J.D., Wood, A.D., Polys, N.F., Yuan, X., 2014a. The Weng'an biota and the Ediacaran radiation of multicellular eukaryotes. National Science Review 1, 498–520.
Xiao, S., Narbonne, G.M., Zhou, C., Laflamme, M., Grazhdankin, D.V., Moczydłowska-Vidal, M., Cui, H., 2016. Toward an Ediacaran time scale: problems, protocols, and prospects Episodes: (in press).
Xiao, S., Schiffbauer, J.D., McFadden, K.A., Hunter, J., 2010. Petrographic and SIMS pyrite sulfur isotope analyses of Ediacaran chert nodules: implications for microbial processes in pyrite rim formation, silicification, and exceptional fossil preservation. Earth and Planetary Science Letters 297, 481–495.
Xiao, S., Shen, B., Zhou, C., Xie, G., Yuan, X., 2005. A uniquely preserved Ediacaran fossil with direct evidence for a quilted bodyplan. Proceedings of the National Academy of Sciences of the United States of America 102, 10227–10232.
Xiao, S., Zhang, Y., Knoll, A.H., 1998. Three-dimensional preservation of algae and animal embryos in a Neoproterozoic phosphorite. Nature 391, 553–558.
Xiao, S., Zhou, C., Liu, P., Wang, D., Yuan, X., 2014b. Phosphatized acanthomorphic acritarchs and related microfossils from the Ediacaran Doushantuo Formation at Weng'an (South China) and their implications for biostratigraphic correlation. Journal of Paleontology 88, 1–67.
Xu, H., 2010. Synergistic roles of microorganisms in mineral precipitates associated with deep sea methane seeps. In: Barton, L.L., Mandl, M., Loy, A. (Eds.), Geomicrobiology: Molecular and Environmental Perspective. Springer, Berlin, Germany, pp. 325–346.
Yeh, L., Sun, S., Chen, Q., Guo, S., 1986. Proterozoic and Cambrian Phosphorites deposits: Kunyang, Yunnan, China., Phosphate Deposits of the World. Proterozoic and Cambrian Phosphorites vol. 1 pp. 149–154.
Yin, Z., Zhu, M., Davidson, E.H., Bottjer, D.J., Zhao, F., Tafforeau, P., 2015. Sponge grade body fossil with cellular resolution dating 60 Myr before the Cambrian. Proceedings of the National Academy of Sciences 112, E1453–E1460.
Zhang, H., Xiao, S., Liu, Y., Yuan, X., Wan, B., Muscente, A., Shao, T., Gong, H., Cao, G., 2015. Armored kinorhynch-like scalidophoran animals from the early Cambrian. Scientific Reports 5, 16521.
Zhou, C., Xiao, S., 2007. Ediacaran $\delta^{13}C$ chemostratigraphy of South China. Chemical Geology 237, 89–108.
Zhou, C., Brasier, M.D., Xue, Y., 2001. Three-dimensional phosphatic preservation of giant acritarchs from the terminal Proterozoic Doushantuo Formation In Guizhou and Hubei Provinces, South China. Palaeontology 44, 1157–1178.
Zhu, M., Zhang, J., Yang, A., 2007. Integrated Ediacaran (Sinian) chronostratigraphy of South China. Palaeogeography, Palaeoclimatology, Palaeoecology 254, 7–61.
Zhu, M., Lu, M., Zhang, J., Zhao, F., Li, G., Yang, A., Zhao, X., Zhao, M., 2013. Carbon isotope chemostratigraphy and sedimentary facies evolution of the Ediacaran Doushantuo Formation in western Hubei, South China. Precambrian Research 225, 7–28.